ELSEVIER

Contents lists available at ScienceDirect

Smart Agricultural Technology

journal homepage: www.journals.elsevier.com/smart-agricultural-technology





Tree-level citrus yield prediction utilizing ground and aerial machine vision and machine learning

Vinay Vijayakumar, Yiannis Ampatzidis*, Lucas Costa

Agricultural and Biological Engineering department, Southwest Florida Research and Education Center, University of Florida, IFAS, 2685 SR 29 North, Immokalee, FL 34142. USA

ARTICLE INFO

Keywords: Artificial intelligence Precision agriculture Remote sensing, UAV

ABSTRACT

Yield prediction of citrus provides critical information before harvest to growers and allied industry to predict the resources required for workers, storage, and transportation of the harvest. In this study, three machine learning (ML) based models were developed for tree-level citrus yield prediction: (i) Model-1 utilized UAV imagery; (ii) Model-2 utilized UAV imagery and ground-based fruit detection and counts from images taken from one side of the tree; and (iii) Model-3 utilized UAV imagery and ground-based fruit detection and counts from images taken from two sides of the tree. The UAV images were used as input to a novel cloud-based technology, Agroview, to get the tree health, height, and canopy area information. The multispectral bands and the tree structural parameters were the input for Model-1. Two images per tree were captured from the ground using an RGB camera (one from each side) and were used for fruit count using an object detection algorithm, YOLOv3. Harvest data was collected manually per tree (fruit count and weight). Four ML algorithms - gradient boosting regression (GBR), random forest regression (RFR), linear regression (LR), and partial least squares regression (PLSR) were used to generate the models. Model-2 (MAPE of 23.45%) performed similarly to Model-3 (MAPE of 25.72%) and significantly better than Model-1 (MAPE of 35.59%). Model-2 was selected as the best model because of its low MAPE value in predicting yield at the tree level, and data collection simplicity (compared to Model-3).

1. Introduction

The citrus industry in Florida contributes billions of dollars to its economy every year through citrus fruit production, citrus juice manufacturing, and fresh citrus marketing [15]. Yield prediction is critical in defining adequate management strategies and logistics related to the workforce, storage, packaging, and transportation [5] associated with citrus production. The most widely adopted method for gathering information about yield and fruit size is actual harvesting, weighing, and sorting either by human workforce or commercial grading machines [1, 4,7]. A major drawback of using actual harvest data for yield mapping is the aggregation of the fruit count over spatial areas or times based on the varying spatial and/or temporal aspects of the harvesting processes and techniques [34]. In Florida, a common method for yield prediction of citrus orchards before harvest involves sampling a fixed number of trees (containing immature fruit) from a block, counting the total number of fruits in those trees, and using it to extrapolate for the whole block considering the fruit drops for that season. Fruit drop is nature's way to prevent overproducing. However, it could also be due to stress experienced by the trees because of the scarcity of water, lack of nitrogen in the soil, disease stress (e.g., Huanglongbing), or dry windy weather [8]. This manual yield prediction method is highly error-prone because of the errors involved in extrapolation, random sampling of trees, and the use of a standard fruit drop index or percentage issued by the Florida state (e.g., fruit loss adjustment standard).

Advances in technology and the availability of low-cost UAVs and sensing systems over the past fifteen years have opened up new avenues for researchers to utilize machine vision systems (e.g., spectral and thermal imaging) for high-throughput phenotyping and yield estimation in specialty crops. Maimaitijiang et al., [23] found that instead of using single sensors for determining features, a combination of canopy spectral information and thermal information from multiple sensors resulted in better soybean biochemical parameter estimations. Researchers have also shown that combining thermal canopy information with spectral and structural information improved yield prediction under different weather conditions and development stages of spring barley [31]. Different vegetation indices derived from satellite imagery have been used by researchers to develop a yield prediction model for corn. They

E-mail address: i.ampatzidis@ufl.edu (Y. Ampatzidis).

^{*} Corresponding author.

were compared with machine learning (ML) techniques such as support vector machines (SVM) and multiple regression (MR). It was determined that random forest regression was the most accurate approach for predicting the in-field variability [19]. Kayad et al. [19] also concluded that the ML models produced more robust results than the vegetation indices approach when applied to cornfields. Costa et al. [14] also developed ML based models for predicting grain yield and related traits in wheat with high accuracy by utilizing hyperspectral imaging. Deep learning (DL) has gained much popularity in the past decade with applications in data fusion [26], remote sensing for multi-modal multi-temporal data fusion [9], and countless other applications [13,27,28]. However, the application of DL for yield prediction has been relatively recent. Kuwata & Shibasaki [22] developed deep neural networks (DNNs) to estimate county-level corn yield for the entire area of the United States. It was determined that neural network-trained estimation methods performed feature extraction better than an existing ML algorithm. Wang et al. [36] utilized DL techniques to predict soybean crop yields in Argentina and subsequently used the pre-trained model to predict Brazil soybean harvests using transfer learning. DNNs when applied on a dataset containing the genotype and yield performance of maize hybrids planted between 2008-2016 to predict the yield for 2017 resulted in high prediction accuracy (12% RMSE as compared to the average yield) [20].

In-field machine vision and tree spectral index correlation determined from satellite imagery can also estimate the preharvest fruit load index of mango orchards [6]. Using big-data mining methodologies for yield prediction has gained popularity for crops such as sugarcane. Everingham et al., [18] used the random forest regression method to explain annual variation in regional sugarcane yields using seasonal climate prediction indices, observed rainfall, minimum and maximum temperatures and radiation as input to the classifier model. Despite the increased use of machine vision in agriculture for yield mapping, researchers stress the need for a robust algorithm with a correction factor based on tree health, tree species, canopy size, and tree vigor [34]. A combination of a correction factor based on the ratio of the human count of fruits in images of two sides of sample trees and a hand harvest count of all fruits, and fruit detection using a customized object detection algorithm-YOLO, has also been employed by researchers to estimate yield in mangoes [21]. However, using a single correction factor based on a small number of sample trees resulted in a high total fruit estimation error (17%) in some cases. Sarron et al. [33] utilized tree structure estimates and load index as input variables for tree production estimations and obtained a good correlation (R² greater than 0.77) when evaluated with measured production on 60 trees. Diennevan et al. [17] used UAV RGB image-based models to predict yield of coffee trees using ML algorithms. The UAV data along with the actual yield values were used to determine the most important features and months for yield prediction.

Airborne hyperspectral imagery has been used to estimate canopy features used as input variables for developing yield prediction models for citrus [38,39]. Ye et al. [38] combined two-band vegetation index (TBVI) and canopy size to obtain a model that explained 76.38% of the yield variability among individual citrus trees. But the high dimensionality of the hyperspectral data added to the cost and complexity of the process, limiting the use of the model. Ye et al. [39] also showed that using partial least squares (PLS) models to predict yield based on canopy features was a better alternative to using vegetation indices based on the spectral bands (red, green, blue, and near infrared-NIR). Zaman et al. [40] found a significant correlation (R²) between ultrasonically-sensed tree sizes and fruit yield. They attributed the lower correlation between actual and predicted yield ($R^2 = 0.42$) to poor flowering and fruit drop which do not affect the canopy volume. Machine learning techniques have been implemented in combination with a regression tree model to classify orchards and identify the variables affecting the production by each tree to predict citrus orchard production [16]. Diaz et al. (2017) found that tree age was the most informative variable affecting tree production followed by between and within rows distance. Fruit

count estimation has been done using RGB, NIR, and depth images for immature citrus fruits using machine vision techniques such as circular object detection and classification [12]. Wang et al. [36] detected and counted immature citrus fruits on images based on local binary patterns (LBP) feature using illumination-normalized images. Zhang et al. [41] developed an image segmentation technique to detect and count citrus fruit on images and compare this technique with human vision-based counting obtaining a R² of 0.98 and a detection accuracy of 91.8%. However, these studies focused only on the image processing side of fruit detection and counting, without providing any actual yield prediction numbers for individual trees and blocks. To our knowledge, no other work has combined UAV and ground-based imaging to generate accurate yield prediction models (and not just fruit counts from images), at a tree level, utilizing machine learning for citrus.

This study developed three ML-based models for citrus yield prediction (at a tree level): (i) Model-1 utilized UAV imagery; (ii) Model-2 utilized UAV imagery, ground-based fruit detection and counts from images taken from one side of the tree; and (iii) Model-3 utilized UAV imagery, ground-based fruit detection and counts from images taken from two sides of the tree. Four ML algorithms were used to generate the models: gradient boosting regression (GBR), random forest regression (RFR), linear regression (LR), and partial least squares regression (PLSR). By comparing and evaluating these three models, the best model was selected, which can predict individual tree yield (and yield at a block level) with minimum error and reduce the yield estimation errors associated with the manual sampling and estimation method, which is the currently used method in Florida citrus industry.

2. Materials and methods

2.1. Experimental design

In this study, three yield prediction models, each using different data structures, were generated and compared. The first model (Model-1) was based on spectral data collected from UAV multispectral imaging. The multispectral and RGB data captured from a UAV were then processed and stitched in Pix4d (Pix4D, Lausanne, Switzerland) to create an orthomosaic uploaded to a novel cloud-based technology, Agroview [2, 3], to generate individual tree structural information like tree height, canopy area, and tree health/stress data. For the second and third yield prediction models (Model-2 and Model-3), a hand-held camera (Canon EOS 5D, Tokyo, Japan) was used to take images of the trees from the east and west side of the rows. A deep learning-based object detection algorithm, YOLO version 3 [30], was used on these images to detect and count fruit, which was used in addition to the UAV and tree structural data as input parameters for the machine learning algorithms to generate Model-2 and Model-3. Model-2 used fruit count from images captured from one side of the tree, while Model-3 used fruit count from images taken from both sides (front and back of tree) of the tree. The yield prediction, at a tree level, from all three models were compared to the actual harvest count of 48 trees (collected in the first quarter of 2020, a week after the spectral and image data collection). The accuracy of the yield estimation per tree was evaluated for all three models using the mean absolute percentage error (MAPE) and the best machine learning algorithm was selected. Fig. 1 presents the workflow of this study.

2.2. Study site

An area on a citrus farm (Lat 26° 27'47" N, Long 81°26'35" W) within the University of Florida's Southwest Florida Research and Education Center premises was chosen as the study site. The selected block had more than 100 trees (Hamlin, Citrus Sinensis), mostly healthy, with varying canopy area and fruit density, and 48 trees out of these 100 were chosen for this study. All data (e.g., UAV, ground-taken images for object detection, and harvest counts) were collected in the third and fourth

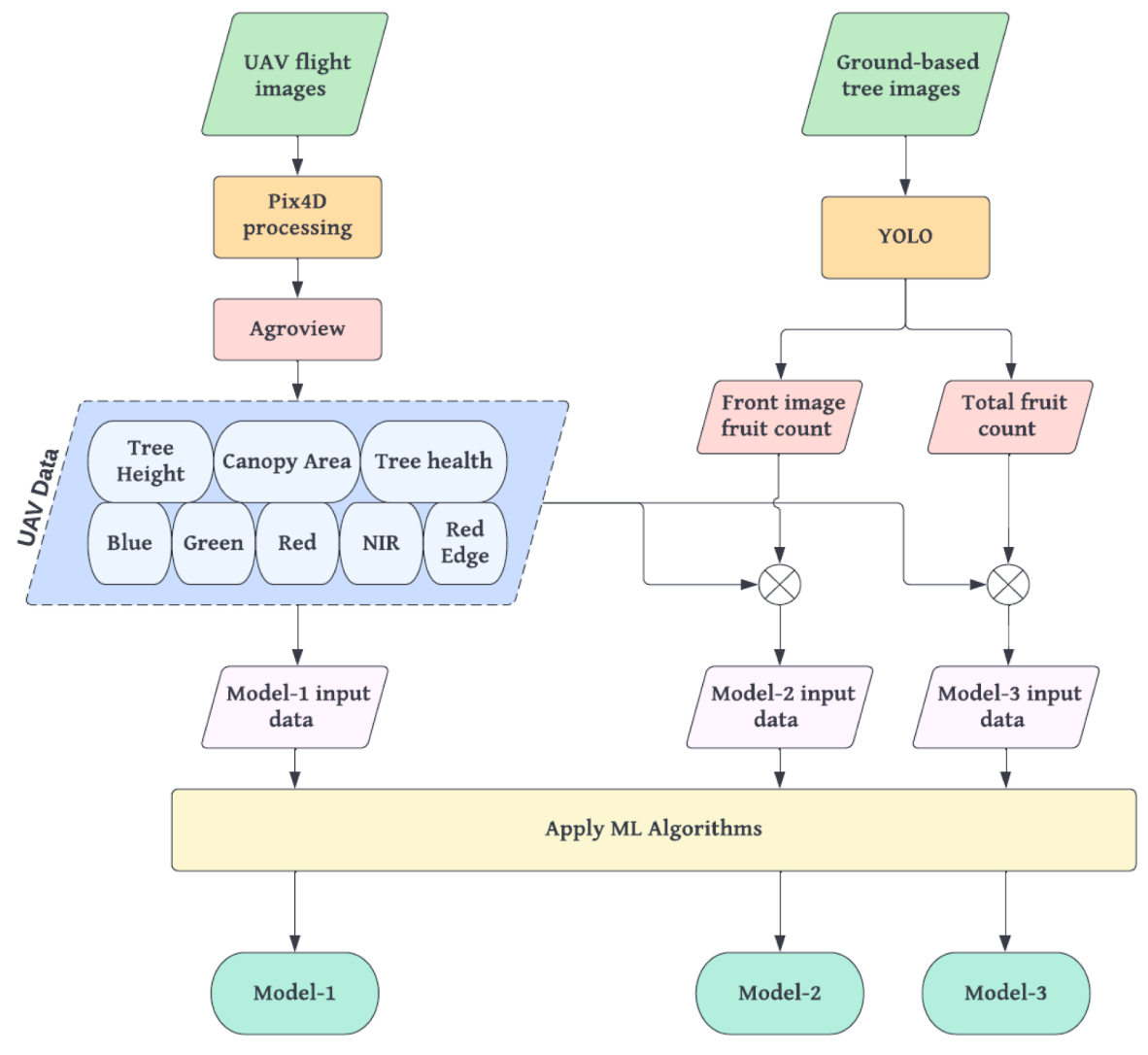


Fig. 1. Workflow of the study.

week of March 2020.

2.3. UAV imagery acquisition

A DJI Phantom 4 Pro+ (Shenzen, China) drone was flown at 122 m (400 ft) for image acquisition in the third week of March 2020 around noon time, when the intensity of sunlight was moderate. An RGB camera (Phantom 4 Pro+ camera, DJI, WA) attached to the Phantom Pro+ and a multispectral camera (RedEdge-M, Micasense, WA, USA) were used to obtain the required data. For the RGB camera, a front overlap of 80% and a side overlap of 70% were set on the Pix4DMapper app. For the multispectral camera, an overlap of 80% was set for both front and side overlap.

2.4. UAV data processing

Data processing was done using the Pix4DMapper software (Pix4D S. A., Prilly, Switzerland). The collected UAV images were stitched together to get the aerial maps for each of the following bands: red (R), green (G), blue (B), red edge, and near-infrared (NIR). The tree height, tree health, and canopy area were extracted from the stitched images using Agroview [3]. Agroview is a cloud and AI-based application used for surveying and assessing agricultural fields by processing, analyzing, and visualizing the data cost-effectively collected from UAVs. For example, Agroview was used as a high-throughput phenotyping tool for

the evaluation of citrus rootstock varieties in large-scale experiments [2]. Agroview is able to estimate the tree height and canopy area with an accuracy of 95.53% and 86.12%, respectively [3].

2.5. Ground fruit detection and count

Two images were taken per tree, from west and east views (Fig. 3), using a Canon EOS 5D (Tokyo, Japan) camera, in the third week of March 2020. The images were taken between 12 PM - 2 PM and between 5 PM - 6 PM to prevent direct glare from the sun. The intensity of sunlight was higher for the images taken at noon than those taken at 5 PM. The front side images were taken standing in the center of the block between two rows of trees (3.8 m from the center of the trees), while the backside images were taken from the adjacent block of trees (5.4 m from the center of the trees of the current block). These images were separated into training and testing blocks (80/20 split). A labeling software called LabelMe [32] was used for annotation of the citrus fruits in the images. Post-annotation, the images were used for training the ML models. A weight file, trained previously on immature citrus fruits, was used for training [37]. The state-of-the-art object detection algorithm -YOLO (version 3) was used for fruit detection (e.g., Fig. 4). The fruit detection using YOLO v3 was carried out for both sides of the tree. This number (fruit counts per tree) was used as an input parameter for the yield prediction models Model-2 and Model-3. All the 48 trees were manually harvested and the fruit count for each tree was recorded.



Fig. 2. UAV image of the study site with the blue border showing the experimental trees.

2.6. Machine learning implementation and models

2.6.1. k-fold cross-validation

The k-fold cross-validation is a popular data resampling method implemented on machine learning models to get a less biased model estimation. In k-fold cross-validation, a given data sample is split into k' number of groups. This allows each sample to be in the hold-out set 1 time and to be used to train the model k-1 times [11]. k=5 and k=10 are the most commonly chosen values for k-fold cross-validation, and the former was selected for our model.

2.6.2. Regression models

The gradient boosting regression (GBR), random forest regression (RFR), linear regression (LR), and partial least squares regression (PLSR) methods were used to generate yield prediction models for the dataset. The GBR produces a predictive model from an ensemble of weak predictive models [35]. It involves three elements: a loss function that is

optimized, a weak learner which is generally a decision tree constructed in a 'greedy' manner, and finally, an additive model, which uses a gradient descent procedure to minimize the losses when adding trees [10]. Not only does GBR provide great predictive accuracy, but it also works well without any data pre-processing and missing data. The RFR is a robust algorithm involving an ensemble of decision trees constructed randomly. Each tree makes its prediction, averaged out to produce a single result [25]. The LR is one of the simplest and most popular regression models used in statistical modeling. Its popularity stems from the fact that it can be used satisfactorily for small sample sizes and the results obtained from linear regression are easy to interpret. Linear regression captures the dependencies between the inputs and outputs through an estimated linear function defined by the predicted weights [29]. The PLSR is used to model a response variable when many predictor variables are involved. It is handy when the predictors are highly collinear or when the number of predictors exceeds the number of observations. In such cases, it is better than the ordinary least-squares method, which either fails or generates coefficients with high standard errors [24].

A script including all four algorithms was run using 'harvest count' as the objective function (the value that the ML algorithm is trying to estimate). Model-1 used multispectral data and tree structural data as its input parameters. Model-2 used fruit count from one side of the tree and Model-3 used fruit count from both sides of the tree in addition to the input parameters of Model-1 (Table 1).

2.6.3. Evaluation metrics

The performance of the object (fruit) detection algorithm YOLO v3 was evaluated using precision, recall, and F1 score. Precision and recall are calculated using True Positives (TP), False Positives (FP), and False Negatives (FN). For the detection of citrus fruits on images, FN represents the number of times the algorithm missed detecting a fruit in a particular image, FP represents the number of times the algorithm detected non-fruit as fruits, and TP is the number of times the algorithm correctly detected a fruit.

$$Precision = \frac{True \ Positive}{True \ Positive \ + False \ Positive}$$
 (1)

$$Recall = \frac{True\ Positive}{TruePositive + FalseNegative}$$
 (2)

$$F1 \ score = 2 * \frac{Precision * Recall}{Precision + Recall}$$
 (3)

The mean absolute percentage error was used as an evaluation metric for the ML yield prediction models. It is a commonly used key performance index (KPI). Essentially, it gives an average of the percentage error. It is given by Eq. 4.

$$MAPE = \frac{1}{n} \sum \left| \frac{Y - \widetilde{Y}}{Y} \right| \tag{4}$$

where, Y= actual value of the target parameter (in this case, it is the actual harvest count of the tree), $\tilde{Y}=$ value of the target parameter estimated from the ML algorithms, n= sample size, (| |) = absolute value, and \sum = summation operator.

3. Results

3.1. Accuracy of the fruit detection model

For the fruit detection on images, YOLO v3 gave a high overall precision of 0.96, indicating that the algorithm is highly accurate when it detects an object as citrus fruit. An overall recall of 0.83 and an average F1 score of 0.88 suggests that the trained detection model is quite robust (Table 2).



Fig. 3. A citrus tree row with the arrows showing the side of the tree considered front and backside for capturing ground-based images.

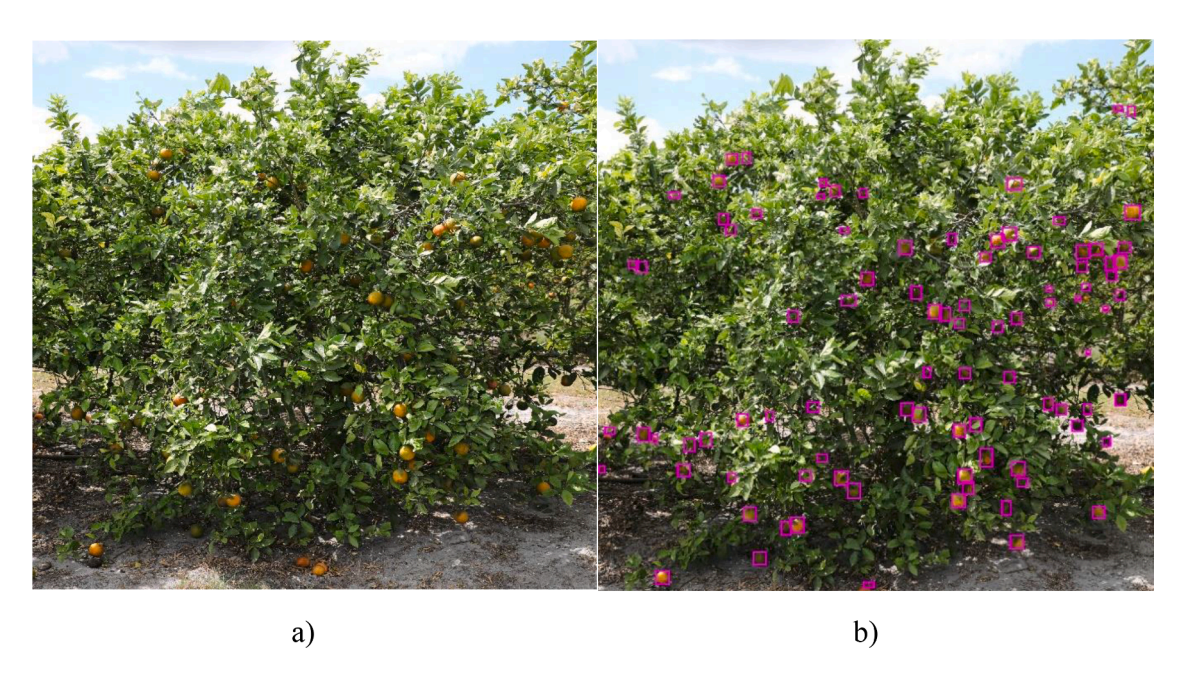


Fig. 4. a) Original ground-based RGB image taken using a Canon camera. b) Fruit detection using YOLO applied on the same image.

Table 1
Description of the objective function and input data for each model

	Model-1	Model-2	Model-3
Objective function	Harvest count	Harvest count	Harvest count
Input parameters	Multispectral data Tree structural data	Multispectral data Tree structural data 1-sided fruit count	Multispectral data Tree structural data 2-sided fruit count

Table 2Precision, recall, and F1 score of the object detection algorithm for the tree images.

	Row-1	Row-2	Overall
Precision	0.96	0.96	0.96
Recall	0.80	0.86	0.83
F1 score	0.87	0.90	0.88

3.2. Machine Learning models applied for yield estimation

The three models developed in this study were compared using the average MAPE for each of the four ML algorithms used. Boxplots were created for each model. Table 3 presents the complete dataset for 48 trees. The first column shows the yield per tree which is the number of fruits harvested from each tree. The columns 2-6 show the multispectral data of each tree obtained from UAV flights. Columns 7-9 show the tree structural parameters (tree height and canopy area) along with a health index (acquired by Agroview). The machine vision count columns present the fruit count from the front side and both sides of the tree. The yield estimated by Model-1, Model-2, and Model-3 for each of the trees is presented in columns 12-14.

Model-1

Model-1, where the UAV-based data (spectral data and tree structural parameters) were the only inputs to the ML algorithms, was evaluated using average MAPE. The average MAPE for each algorithm for each k-fold validation is presented in Table 4.

For Model-1, the average MAPE for all the ML algorithms was above 35%. The LR gave the best yield estimate (MAPE of 35.59 %; Table 4)

•

Smart Agricultural Technology 3 (2023) 1000/

 Table 3

 Complete dataset with UAV data, machine vision-based fruit count, yield estimate, missing fruit, and absolute percentage error of all three models.

Part	Harvest Count	Multisp	ectral Dat	a			Tree Str Paramet			Machine V	ision Count	Yield Esti	imate		Missing f	ruit		Absolute	Percentage	e Error
244 247		Blue	Green	Red	R Edge	NIR			Health										Model- 2	Model-
195 42,65 72,69 42,79 103,60 13,10 83 121,3 0.89 0.0 163 219,50 122,20 21,30 21,30 21,50 84 94 11,10 222 13,50 135 131 81,1 98 14 21,50 22 13,1 13,1 33,1 33,1 33,1 33,3 33,3 33,3 22 23 41,2 11,1 33,3 38,3 23,1 33,3 33,3 32,2 11,1 33,3 38,3 27,7 13,1 33,3 34,2 31,3 31,3 38,3 27,7 13,1 33,3 31,3 38,3 27,7 31,3 33,3 31,3 33,3 32,7 33,3 31,3 33,3 31,3 33,3 31,2 33,3 31,3 33,3 31,3 33,3 31,3 33,3 31,3 33,3 31,3 33,3 31,3 33,3 31,3 33,3 33,3 33,3 33,3 33,3 33,3	228	35.23	61.74	36.44	99.44	135.19	8.3	153.8	0.9	72	155	316.92	275.93	272.11	-89	-48	-44	39	21.02	19.35
100	204	42.79	69.07	43.35	100.64	128.52	8.2	116.2	0.92	57	123	208.68	163.48	156.45	-5	41	48	2.29	19.86	23.31
	195	42.65	72.69	42.79	103.67	131.76	8.3	121.3	0.89	60	163	219.67	172.28	213.78	-25	23	-19	12.65	11.65	9.63
	160	43.7	74.54	47.05	102.18	126.05	9.2	116.2	0.94	111	222	294.56	314.53	307.25	-135	-155	-147	84.1	96.58	92.03
412 49.38 69.99 37.88 101.8 191.9 8 14.98 91.9 100 23 21.00 23.38 104.0 93.55 11.82 8.4 13.90 11.5 25.5 21.00 10.90 12.2 22.5 13.00 10.00 12.00 20.10 20.10 20.10 23.80 72.00 11.0 49 37.00 0.0 87 43.78 60.50 30.20 151.8 11.0 121.3 12.0 12.0 11.0 12.0 11.0 12.0 11.0 12.0 11.0 12.0 11.0 19.0 12.0 11.0 19.0 12.0 11.0 19.0 12.0 11.0 19.0 18.0 11.0 19.0 18.0 11.0 19.0 10.0	61	47.33	81.33	47.88	114.7	138.18	9.5	86.8	0.86	36	84	76.32	41.06	47.88	-15	20	13	25.11	32.69	21.51
	442	34.34	66.85	37.22	101.77	119.85	9.3	171	0.93	122	258	424.82	430.59	429.14	17	11	13	3.89	2.58	2.91
190 34,49 65,27 36,12 93,55 118,48 91,00 121,00 92,00 61 190,00 21,62 201,62 201,62 201,62 201,60 201,00 <		34.38						148.2		100		342.02		348.33		98	64		23.82	15.45
387 89.02 36.26 15.15 11.62 9.1 12.13 0.9 12.8 22.5 193.24 30.70 26.99 19.4 84 12.3 50.70 21 286 33.24 66.31 38.81 105.28 12.74 82.1 11.62 0.9 82 176 20.16 21.15 78 44 47 22.22 23 22 26 15.2 30.5 41.2 30.3 31.8 42 11.2 30.9 14.2 10.2 22 11.2 10.2 21.2 12.2 <td>362</td> <td>35.41</td> <td>69.87</td> <td>37.85</td> <td>104.2</td> <td>126.57</td> <td>8.7</td> <td>126.6</td> <td>0.93</td> <td>115</td> <td>235</td> <td>261.46</td> <td>312.97</td> <td>308.62</td> <td>101</td> <td>49</td> <td>53</td> <td>27.77</td> <td>13.54</td> <td>14.75</td>	362	35.41	69.87	37.85	104.2	126.57	8.7	126.6	0.93	115	235	261.46	312.97	308.62	101	49	53	27.77	13.54	14.75
87 38,88 55,42 38,34 13,34 13,36 13,86 19,2 101,1 0,93 41 139 25,39 11,76 21,37 48,4 1,27 19,18 92 176 31,19 67,37 36,20 106,66 13,14 8.8 121,3 0,91 86 192 227,12 23,75 245,65 5.1 60 70 20,03 33 18 4,224 33,28 31,44 8,22 12,43 0,91 86 19 11,44 14,64 14,69 16,59 10 60 50 47,02 33 31,44 62,24 33,23 10,17 13,28 11,04 11,04 11,44 14,62 14,72 10 20 26,65 30,73 16,76 30 41,14 13,28 10 11,22 20 12,22 11,23 13,23 10 41,22 12,22 11,23 13,23 10 42,22 22,23 10 <th< td=""><td>190</td><td>34.49</td><td>65.27</td><td>36.12</td><td>95.35</td><td>118.43</td><td>8.4</td><td>131.9</td><td>0.92</td><td>61</td><td>169</td><td>261.62</td><td>201.45</td><td>238.66</td><td>-72</td><td>-11</td><td>-49</td><td>37.69</td><td>6.03</td><td>25.61</td></th<>	190	34.49	65.27	36.12	95.35	118.43	8.4	131.9	0.92	61	169	261.62	201.45	238.66	-72	-11	-49	37.69	6.03	25.61
286 33,24 66,31 35,281 10,282 12,749 82 116,2 0.9 82 176 20,166 211,768 211,768 21,722 22,722 22,722 22,722 22,722 22,722 22,722 22,722 22,722 22,722 22,722 20,722 10,722 22,722 2	387	34.78	69.02	36.26	105.15	116.82	9.1	121.3	0.9	128	225	193.24	302.76	263.99	194	84	123	50.07	21.77	31.79
176 34 19 67.37 36.64 98.8 11.48 8.8 121.3 0.9 86 192 227.12 237.12 245.65 1.51 62 70 290.8 33.13 126 31.14 62.24 33.95 104.21 130.00 10.4 106.1 0.92 56 119 226.65 16.24 14.97 1.00 36 2.4 79.09 22.3 30.3 28.97 83.3 31.83 38.22 124.79 0.92 0.92 16.7 19.2 26.65 16.23 14.19 0.0 3.0 4.0 1.0 9.0 1.0 26.5 1.62 19.73 3.0 2.0 2.0 3.3 1.0 3.0 4.0 1.0 1.0 0.9 1.0 20.2 20.13 20.3 19.1 0.2 2.0 1.0 1.0 1.0 1.0 1.0 1.0 1.0 1.0 1.0 1.0 1.0 1.0 1.0 1.0 1.0	87	36.88	75.42	35.34	113.04	139.68	10.2	101.1	0.93	41	139	253.92	171.47	213.71	-167	-84	-127	191.86	97.09	145.64
216 32,15 62,77 34,46 98,88 117,69 11.3 91.5 0.91 86 194 114.44 14.69 16.59 102 69 50 47.02 23 126 31.14 62.24 33.95 18.33 11.22 12.78 22.31 26.65 30.72 137.69 11.2 60 15 12.02 1.2 195 30.59 61.78 35.08 94.71 12.26 10.11 0.91 100 202 201.33 203.34 197.9 -5 -8 -3 2.63 9.7 190 31.8 64.62 34.2 10.17 141.12 12.6 95.3 0.9 74 146 170.39 19.19 150.85 0 1 9 12.6 68.7 105 191 18.2 190.7 18.77 18.7 18.2 11.1 12.1 12.0 44.6 4.5 4.0 2.0 4.0 4.0 4.5 4.0	286	33.24	66.31	35.81	105.28	127.49	8.2	116.2	0.9	82	176	208.16	211.76	211.58	78	74	74	27.22	25.96	26.02
126 31.14 62.24 33.95 104.21 130.05 104.21 130.05 56 119 225.65 162.34 149.72 -100 -36 -24 79.90 22 12.78 30.29 31.28 31.83 31.83 36.83 31.81 36.22 12.47 10.5 10.1 0.93 69 167 20.422 157.83 177.69 1.12 -66 -86 12.10.93 7.1 150 30.59 61.78 30.59 11.77 11.12 12.6 10.5 10.11 0.91 100 202 200.013 203.34 197.9 5 -8 -3 2.63 4.0 11.93 10.0 20.0 10.0 <th< td=""><td>176</td><td>34.19</td><td>67.37</td><td>36.26</td><td>106.66</td><td>131.45</td><td>8.8</td><td>121.3</td><td>0.9</td><td>86</td><td>192</td><td>227.12</td><td>237.72</td><td>245.65</td><td>-51</td><td>-62</td><td>-70</td><td>29.05</td><td>35.07</td><td>39.57</td></th<>	176	34.19	67.37	36.26	106.66	131.45	8.8	121.3	0.9	86	192	227.12	237.72	245.65	-51	-62	-70	29.05	35.07	39.57
303 98,7 58,33 31.83 98,22 124,78 82,2 142,7 90,2 102 231 266,57 307,21 31,63 36 4 1,5 12,00 1.7 195 33,29 61,78 35,08 94,71 124,74 10,5 10,11 0.91 100 202 200,13 203,34 197,9 -5 -8 3 2,63 4,7 170 31,8 6462 32,00 141,12 12,0 96,3 0,9 74 146 170,00 187,77 162,76 0 2 27 0,04 1.1 250 30,5 6421 33,09 96,61 132,92 9 12,66 887 105 194 238,88 261,35 230,1 11 -11 -11 20,00 4,46 4.4 4,74 4,86 4,4 4,30 4,86 4 4,92 4,46 4,4 4,30 4,50 4,46 4,4 4,2	216	32.15	63.77	34.64	99.8	117.69	11.3	91.5	0.91	86	194	114.44	146.99	165.99	102	69	50	47.02	31.95	23.15
92 33.2 69.63 35.93 101.71 132.86 11.91 101.1 0.9 69 167 204.22 137.88 177.69 -11.2 -66 -86 12.198 7.1 170 31.8 64.62 34.2 10.17 141.12 12.6 96.3 0.9 74 146 170.39 169.19 150.85 0 1 19 0.23 0.0 150 34.62 64.63 38.05 107.69 125.84 11.5 91.5 0.91 19 168 190.07 187.77 162.76 0 2 27 0.04 1.1 124 33.39 71.79 37.78 114.1 132.14 8.3 91.5 0.88 72 148 173.3 169.43 170.85 49 45 -47 39.76 33 288 64.04 67.3 58.82 109.8 131.78 8.2 111.1 0.91 9 124 207.47 165.3	126	31.14	62.24	33.95	104.21	130.05	10.4	106.1	0.92	56	119	225.65	162.34	149.72	-100	-36	-24	79.09	28.84	18.83
195 30,5 61,7 83,08 94,71 124,74 10.5 101.1 0.91 100 202 200,13 203,34 107,9 -5 -8 -3 2.63 4.4 170 31.8 64.62 38.05 107,69 125.84 11.5 91.5 0.91 91 168 190,07 187,77 162.76 0 2 27 0.04 1.1 250 30.5 64.21 33.19 96.61 132.92 9 126.6 0.87 105 194 238.85 261.35 200.1 11 -11 20 4.46 4.2 288 4.60 67.33 108.5 127.61 8.6 131.9 0.92 98 219 294.08 287.91 308.06 -6 0 -20 21.11 0.0 280 41.52 75.35 41.56 108.8 141.27 8.2 11.12 0.91 66 124 0.07 31.33 31.9	303	29.87	58.33	31.83	98.22	124.78	8.2	142.7	0.92	102	231	266.57	307.21	317.63	36	-4	-15	12.02	1.39	4.83
170 31.8 64.62 34.2 101.7 14.12 12.6 95.3 0.9 74 14.6 170.39 169.19 150.85 0 1 19 0.23 0.0 150 34.62 64.21 33.19 96.61 132.92 9 126.60 0.87 105 194 238.85 261.35 230.11 11 -11 20 4.46 4. 124 33.39 71.79 37.78 114.11 132.14 8.3 91.5 0.88 72 148 173.3 169.43 170.85 -49 -45 -47 39.76 38 280 53.43 76.29 98.22 11.14 0.91 69 124 207.47 165.35 162.06 73 115 117 25.9 44 262 42.92 75.73 43.56 108.85 147.28 11.62 0.91 78 167 223.86 237.90 237.96 38 27 24 <td>92</td> <td>33.2</td> <td>69.63</td> <td>35.93</td> <td>101.71</td> <td>132.86</td> <td>11.9</td> <td>101.1</td> <td>0.9</td> <td>69</td> <td>167</td> <td>204.22</td> <td>157.8</td> <td>177.69</td> <td>-112</td> <td>-66</td> <td>-86</td> <td>121.98</td> <td>71.52</td> <td>93.14</td>	92	33.2	69.63	35.93	101.71	132.86	11.9	101.1	0.9	69	167	204.22	157.8	177.69	-112	-66	-86	121.98	71.52	93.14
190 34,62 69,64 38.05 107,69 125,84 11.5 91.5 0,91 168 190,07 187.77 162.76 0 2 27 0.04 1.2 250 30.5 64.21 33.99 96.61 132.14 83.99 1.05 0.88 72 148 173.3 169.43 170.85 .49 .45 .47 39.76 3.36 288 46.04 67.33 50.08 99.65 127.61 8.6 131.9 0.92 98 219 294.08 287.91 308.06 -6 0 -0 20 2.11 0 262 42.92 73.55 44.57 114.68 8.7 116.2 0.94 78 167 223.86 235.09 237.96 38 27 24 145.59 76.2 44.9 41.59 76.7 43.56 10.8 19.4 282.23 38.0 237.96 38 27 24 14.55 76.2 4	195	30.59	61.78	35.08	94.71	124.74	10.5	101.1	0.91	100	202	200.13	203.34	197.9	-5	-8	-3	2.63	4.28	1.49
250 30.5 64.21 33.19 96.61 132.14 8.3 91.5 10.8 194 238.85 26.1.35 23.01 11 -11 20 4,46 4.4 288 46.04 67.33 50.08 99.65 127.61 8.6 131.9 0.92 98 219 294.08 287.91 308.06 -6 0 -20 2.11 0.0 220 280 23.73 16.25.35 16.25 73 115 117 25.9 44 22.26 42.92 73.55 44.57 10.84 114.67 8.7 116.2 0.94 78 167 22.38 235.00 237.96 38 27 24 14.59 44 41.25 63.55 42.16 8.8 114.67 0.94 78 167 22.8 89.23 314.23 331.69 150 125 107 34.12 22.0 48.0 48.2 10.9 11.66 8.7 11.26 0.68 13.4	170	31.8	64.62	34.2	101.77	141.12	12.6	96.3	0.9	74	146	170.39	169.19	150.85	0	1	19	0.23	0.48	11.26
124 33,9 17,79 37,78 11,11 132,14 8.5 91,55 0.88 72 148 17,33 10,43 10,45 4,74 39,76 36,76 32,22 32,22 294,08 28,71 30,80.6 -6 0 -20 21,11 0 0 29,68 21,74 165,35 162,96 73 115 117 25,99 21,40 29,48 287,91 30,80.6 -6 0 -20 21,11 0 0 22,40 28,53 16,26 73 115 117 25,99 31,40 60,90 33 40,74 165,35 162,96 73 115 117 25,90 14,56 16,70 14,56 10,7 22,2 0.91 106 227 289,23 314,23 31,60 15,00 125 14,12 0.91 34 68 83,47 34,91 0.09 39 9 38 89,7 22,2 0.89 110 0.05 232,23	190	34.62	69.46	38.05	107.69	125.84	11.5	91.5	0.91	91	168	190.07	187.77	162.76	0	2	27	0.04	1.17	14.34
288 46,0 67,33 50.08 99,65 127,61 8.6 131,9 0.92 98 219 294,08 287,91 308,06 -6 0 -20 2.11 0.0 280 53,43 76.73 59,82 109,88 11,16 0.91 69 124 207,47 165,35 162,96 73 115 117 25,9 42 439 41,59 76,73 43,56 108,88 144,32 10.5 142,7 0.91 106 227 289,23 314,23 331,69 150 125 107 34,12 236 336 33,42 61,35 42,16 88,9 114,27 0.95 88 194 326,21 302,84 302,54 10 33 33 291 9.2 38 80,11 126,66 9.8 142,7 0.95 88 194 326,21 302,84 304,34 -3 -4 16 1.02 1.02 1.02 1	250	30.5	64.21	33.19	96.61	132.92	9	126.6	0.87	105	194	238.85	261.35	230.1	11	-11	20	4.46	4.54	7.96
280 53,43 76,29 59,82 109,8 117,8 8.2 111,1 091 69 124 207,47 165,35 162,96 73 115 117 25,9 4,45 262 42,92 73,55 44,56 108,88 147,68 8.7 1162 0.94 78 167 223,86 235,09 331,69 150 125 107 341,22 103 18,12 104 14,56 10 44 14,25 63,55 42,16 88.9 14,66 8.7 82,2 0.91 166 88 83,47 34,91 6.09 39 9 38 89.7 22 360 35,5 70,29 38,78 105,11 126,36 9.8 142,7 0.89 110 205 323,25 324,49 304,34 -3 4 16 10,2 1,2 4 16 10,2 1,2 4 16 10,2 1,2 4 16 10,2 1	124	33.39	71.79	37.78	114.1	132.14	8.3	91.5	0.88	72	148	173.3	169.43	170.85	-49	-45	-47	39.76	36.64	37.78
262 42.92 73.55 44.57 108.45 147.68 8.7 116.2 0.94 78 167 223.86 233.09 237.96 38 27 24 14.56 10 439 41.59 76.73 43.56 108.88 144.32 10.5 142.7 0.91 106 227 289.23 314.23 331.69 150 125 107 34.12 22 336 33.42 61.35 34.59 93.15 122.6 10.6 142.7 0.95 88 194 326.21 302.84 302.54 10 33 33 2.91 9.2 270 51.34 75.06 54.82 10.06 11.5 142.7 0.89 110 205 323.25 324.49 304.34 -8 -6 -5 -6 31.31 33 28 129.14 14.57 0.89 110 205 323.25 324.49 304.34 -8 -6 313.31 33 <t< td=""><td>288</td><td>46.04</td><td>67.33</td><td>50.08</td><td>99.65</td><td>127.61</td><td>8.6</td><td>131.9</td><td>0.92</td><td>98</td><td>219</td><td>294.08</td><td>287.91</td><td>308.06</td><td>-6</td><td>0</td><td>-20</td><td>2.11</td><td>0.03</td><td>6.97</td></t<>	288	46.04	67.33	50.08	99.65	127.61	8.6	131.9	0.92	98	219	294.08	287.91	308.06	-6	0	-20	2.11	0.03	6.97
439 41.59 76.73 43.56 108.88 144.32 10.5 142.7 0.91 106 227 289.23 314.23 331.69 150 125 107 34.12 284 44 41.25 63.55 42.16 88.9 114.66 8.7 82.2 0.89 34 68 83.47 34.91 6.09 .39 9 38 89.7 22 320 36.5 70.29 38.78 105.11 126.36 9.8 142.7 0.89 110 205 323.25 324.49 304.34 -3 -4 16 1.02 1. 274 51.34 75.06 54.82 100.46 115.09 11.5 142.7 0.88 126 225 359.8 362.44 304.34 -3 -4 16 1.02 1. 274 51.34 75.06 54.82 100.4 11.8 183.8 189 135 250 374.19 419.06 304	280	53.43	76.29	59.82	109.8	131.78	8.2	111.1	0.91	69	124	207.47	165.35	162.96	73	115	117	25.9	40.95	41.8
44 41.25 63.55 42.16 88.9 114.66 87 82.2 0.89 34 68 83.47 34.91 6.09 -39 9 38 89.7 20 336 33.42 61.35 34.59 93.15 122.6 10.6 142.7 0.95 88 194 326.21 302.84 302.54 10 33 33 2.91 9.3 274 51.34 75.06 54.82 100.46 115.09 11.5 142.7 0.88 126 225 359.8 369.24 337.43 -86 -95 -63 31.31 34 368 45.22 73.2 46.52 102.7 129.46 11.8 153.8 0.89 135 250 374.19 419.06 391.65 6 -51 -24 1.68 12 211 36.47 68.61 37.11 10.71 14.17 8.1 150.1 99 193 286.97 301.07 283.75	262	42.92	73.55	44.57	108.45	147.68	8.7	116.2	0.94	78	167	223.86	235.09	237.96	38	27	24	14.56	10.27	9.18
44 41.25 63.55 42.16 88.9 114.66 87 82.2 0.89 34 68 83.47 34.91 6.09 -39 9 38 89.7 20 336 33.42 61.35 34.59 93.15 122.6 10.6 142.7 0.95 88 194 326.21 302.84 302.54 10 33 33 2.91 9.3 274 51.34 75.06 54.82 100.46 115.09 11.5 142.7 0.88 126 225 359.8 369.24 337.43 -86 -95 -63 31.31 34 368 45.22 73.2 46.52 102.7 129.46 11.8 153.8 0.89 135 250 374.19 419.06 391.65 6 -51 -24 1.68 12 211 36.47 68.61 37.11 10.71 14.17 8.1 150.1 99 193 286.97 301.07 283.75	439	41.59	76.73	43.56	108.88	144.32	10.5	142.7	0.91	106	227	289.23	314.23	331.69	150	125	107	34.12	28.42	24.44
336 33.42 61.35 34.59 93.15 122.6 10.6 142.7 0.95 88 194 326.21 302.84 302.54 10 33 33 2.91 92.3 320 36.5 70.29 38.78 105.11 126.36 9.8 142.7 0.89 110 205 323.25 324.49 304.34 -3 -4 16 1.02 1.2 274 51.34 75.06 54.82 100.46 11.5 142.7 0.88 126 225 359.8 369.24 337.43 -86 -95 -63 31.31 34 368 45.22 73.2 46.52 102.7 129.46 11.8 153.8 0.89 135 250 374.19 419.06 391.65 -6 -51 -24 1.68 13 211 36.47 68.61 37.41 107.71 41.17 8.1 106.1 0.92 66 135 169.65 183.41					88.9		8.7			34						9	38		20.66	86.16
320 36.5 70.29 38.78 105.11 126.36 9.8 142.7 0.89 110 205 323.25 324.49 304.34 -3 -4 16 1.02 1.2 274 51.34 75.06 54.82 100.46 115.09 11.5 142.7 0.88 126 225 359.8 369.24 337.43 -86 -95 -63 31.31 33 368 45.22 73.2 46.52 102.7 129.46 11.8 153.8 0.89 135 250 374.19 419.06 391.65 -6 -51 -24 1.68 12 211 36.47 68.61 37.41 107.71 141.71 8.1 106.1 0.92 66 135 169.65 183.41 174.86 41 28 36 19.6 13 268 31.97 71.44 33.3 10.1 131.9 0.93 12 252 251.8 361.24 350.97		33.42	61.35	34.59	93.15	122.6	10.6	142.7	0.95	88	194	326.21	302.84	302.54	10	33	33	2.91	9.87	9.96
274 51.34 75.06 54.82 100.46 115.0 142.7 0.88 126 225 359.8 369.24 337.43 -86 -95 -63 31.31 34 368 45.22 73.2 46.52 102.7 129.46 11.8 153.8 0.89 135 250 374.19 419.06 391.65 -6 -51 -24 1.68 13 211 36.47 68.61 37.41 107.71 141.71 8.1 106.1 0.92 66 135 169.65 183.41 174.86 41 28 36 19.6 11.6 10.9 193 286.97 301.07 283.75 -19 -33 -16 7.08 12 409 34.51 67.87 35.3 108 135.76 10.1 131.9 0.93 192 252 251.8 361.24 350.97 157 48 58 38.44 11 28 31 17.4 11.3 41.0 <t< td=""><td></td><td></td><td></td><td></td><td></td><td></td><td></td><td></td><td></td><td></td><td></td><td></td><td></td><td></td><td></td><td></td><td></td><td></td><td>1.4</td><td>4.89</td></t<>																			1.4	4.89
368 45.22 73.2 46.52 102.7 129.46 11.8 153.8 0.89 135 250 374.19 419.06 391.65 -6 -51 -24 1.68 13 211 36.47 68.61 37.41 107.71 141.71 8.1 106.1 0.92 66 135 169.65 183.41 174.86 41 28 36 19.6 13 268 46.22 70.15 48 95.64 110.13 8.8 131.9 0.93 99 193 286.97 301.07 283.75 -19 -33 -16 7.08 12 409 34.51 67.87 35.3 108 135.76 10.1 131.9 0.93 122 252 251.8 361.24 350.97 157 48 58 38.44 11 286 31.19 71.44 33.95 121.48 146.07 8.7 121.3 0.94 103 208 341.21 369.25 359.75 -55 -83 -74 19.3 292 321							11.5		0.88	126	225					-95	-63		34.76	23.15
211 36.47 68.61 37.41 107.71 141.71 8.1 106.1 0.92 66 135 169.65 183.41 174.86 41 28 36 19.6 135 268 46.22 70.15 48 95.64 110.13 8.8 131.9 0.93 99 193 286.97 301.07 283.75 -19 -33 -16 7.08 12 409 34.51 67.87 35.3 108 135.76 10.1 131.9 0.93 192 252 251.8 361.24 350.97 157 48 58 38.44 11 286 31.19 71.44 33.95 121.48 146.07 8.7 121.3 0.94 103 208 341.21 369.25 359.75 -55 -83 -74 19.3 29 210 44.25 74.49 47.99 101.79 126.86 8.1 73.2 0.86 89 159 66.16 109.76 80.27 54 10 40 44.87 8. 200		45.22		46.52	102.7	129.46	11.8	153.8	0.89	135	250	374.19	419.06		-6	-51	-24	1.68	13.88	6.43
268 46.22 70.15 48 95.64 110.13 8.8 131.9 0.93 99 193 286.97 301.07 283.75 -19 -33 -16 7.08 12 409 34.51 67.87 35.3 108 135.76 10.1 131.9 0.93 122 252 251.8 361.24 350.97 157 48 58 38.44 11 286 31.19 71.44 33.95 121.48 146.07 8.7 121.3 0.94 103 208 341.21 369.25 359.75 -55 -83 -74 19.3 22 321 37.03 69.51 42.14 97.4 111.53 8.2 111.1 0.86 150 353 161.54 284.03 372.27 159 37 -51 49.68 11 120 44.25 74.99 101.79 126.86 8.1 73.2 0.89 86 170 318.44 294.6 286.03 -118 -95 -86 59.22 47 147 31.7									0.92								36	19.6	13.08	17.13
409 34.51 67.87 35.3 108 135.76 10.1 131.9 0.93 122 252 251.8 361.24 350.97 157 48 58 38.44 11 286 31.19 71.44 33.95 121.48 146.07 8.7 121.3 0.94 103 208 341.21 369.25 359.75 -55 -83 -74 19.3 29 321 37.03 69.51 42.14 97.4 111.53 8.2 111.1 0.86 150 353 161.54 284.03 372.27 159 37 -51 49.68 11 120 44.25 74.49 47.99 101.79 126.86 8.1 73.2 0.86 89 159 66.16 109.76 80.27 54 10 40 44.87 8. 200 34.8 71.15 39.39 113.7 135.13 8.2 137.2 0.89 86 170 318.44 294.6 286.03 -118 -95 -86 59.22 44 14 257.96																			12.34	5.88
286 31.19 71.44 33.95 121.48 146.07 8.7 121.3 0.94 103 208 341.21 369.25 359.75 -55 -83 -74 19.3 29 321 37.03 69.51 42.14 97.4 111.53 8.2 111.1 0.86 150 353 161.54 284.03 372.27 159 37 -51 49.68 11 120 44.25 74.49 47.99 101.79 126.86 8.1 73.2 0.86 89 159 66.16 109.76 80.27 54 10 40 44.87 8. 200 34.8 71.15 39.39 113.7 135.13 8.2 137.2 0.89 86 170 318.44 294.6 286.03 -118 -95 -86 59.22 44 11 28 31 75.48 18 19 44.25 14 19.34 44 11 257 148.75 255 239.37 191 85 101 56.25 25 21 24 19.4 <td></td> <td>11.68</td> <td>14.19</td>																			11.68	14.19
321 37.03 69.51 42.14 97.4 111.53 8.2 111.1 0.86 150 353 161.54 284.03 372.27 159 37 -51 49.68 11 120 44.25 74.49 47.99 101.79 126.86 8.1 73.2 0.86 89 159 66.16 109.76 80.27 54 10 40 44.87 8. 120 34.8 71.15 39.39 113.7 135.13 8.2 137.2 0.89 86 170 318.44 294.6 286.03 -118 -95 -86 59.22 47 147 31.7 65.22 34.03 105.17 136.12 8.1 126.6 0.89 48 117 257.96 175.21 177.84 -111 -28 -31 75.48 19 340 31.42 67.34 33.85 107.45 142.53 8.8 121.3 0.84 118 227 148.75 255 239.37 191 85 101 56.25 25 144 32.6 62.48 35.24 91.24 119.34 9.4 121.3 0.91 102 231 237.29 245.69 265.65 -23 -32 -52 10.88 14 1212 31.99 69.75 35.01 104.82 130.96 13.2 126.6 0.9 85 166 319.09 270.76 253.21 -107 -59 -41 50.51 27 148 32.93 71.79 36.24 107.85 137.41 8.1 114.8 0.92 113 181 365.54 392.28 323.16 -100 -126 -57 37.42 47 308 32.36 70.04 36.11 107.82 141.13 11.3 121.3 0.91 80 187 282.66 240.4 257.94 25 68 50 8.23 21																			29.11	25.79
120 44.25 74.49 47.99 101.79 126.86 8.1 73.2 0.86 89 159 66.16 109.76 80.27 54 10 40 44.87 8. 200 34.8 71.15 39.39 113.7 135.13 8.2 137.2 0.89 86 170 318.44 294.6 286.03 -118 -95 -86 59.22 47 147 31.7 65.22 34.03 105.17 136.12 8.1 126.6 0.89 48 117 257.96 175.21 177.84 -111 -28 -31 75.48 19 340 31.42 67.34 33.85 107.45 142.53 8.8 121.3 0.84 118 227 148.75 255 239.37 191 85 101 56.25 25 214 32.6 62.48 35.24 91.24 119.34 9.4 121.3 0.91 102 231 237.29 245.69 265.65 -23 -32 -52 10.88 14 212 <td></td> <td>11.52</td> <td>15.97</td>																			11.52	15.97
200 34.8 71.15 39.39 113.7 135.13 8.2 137.2 0.89 86 170 318.44 294.6 286.03 -118 -95 -86 59.22 47 147 31.7 65.22 34.03 105.17 136.12 8.1 126.6 0.89 48 117 257.96 175.21 177.84 -111 -28 -31 75.48 19 340 31.42 67.34 33.85 107.45 142.53 8.8 121.3 0.84 118 227 148.75 255 239.37 191 85 101 56.25 25 214 32.6 62.48 35.24 91.24 119.34 9.4 121.3 0.91 102 231 237.29 245.69 265.65 -23 -32 -52 10.88 14 212 31.99 69.75 35.01 104.82 130.96 13.2 126.6 0.9 85 166 319.09																			8.53	33.11
147 31.7 65.22 34.03 105.17 136.12 8.1 126.6 0.89 48 117 257.96 175.21 177.84 -111 -28 -31 75.48 19 340 31.42 67.34 33.85 107.45 142.53 8.8 121.3 0.84 118 227 148.75 255 239.37 191 85 101 56.25 25 214 32.6 62.48 35.24 91.24 119.34 9.4 121.3 0.91 102 231 237.29 245.69 265.65 -23 -32 -52 10.88 14 212 31.99 69.75 35.01 104.82 130.96 13.2 126.6 0.9 85 166 319.09 270.76 253.21 -107 -59 -41 50.51 27 190 31.95 67.92 35.49 96.3 116.61 8.1 148.2 0.84 75 156 320.48 234.32 225.33 -130 -44 -35 68.67 23 <td< td=""><td></td><td></td><td></td><td></td><td></td><td></td><td></td><td></td><td></td><td></td><td></td><td></td><td></td><td></td><td></td><td></td><td></td><td></td><td>47.3</td><td>43.01</td></td<>																			47.3	43.01
340 31.42 67.34 33.85 107.45 142.53 8.8 121.3 0.84 118 227 148.75 255 239.37 191 85 101 56.25 25 214 32.6 62.48 35.24 91.24 119.34 9.4 121.3 0.91 102 231 237.29 245.69 265.65 -23 -32 -52 10.88 14 212 31.99 69.75 35.01 104.82 130.96 13.2 126.6 0.9 85 166 319.09 270.76 253.21 -107 -59 -41 50.51 27 190 31.95 67.92 35.49 96.3 116.61 8.1 148.2 0.84 75 156 320.48 234.32 225.33 -130 -44 -35 68.67 23 148 32.93 71.79 36.24 107.85 137.41 8.1 111.1 0.87 49 130 178.12 129.17 145.03 -30 19 3 20.35 12 266 35.03 73.63 37.79 110.4 140.7 8.1 148.2 0.92 113 181 365.54 392.28 323.16 -100 -126 -57 37.42 47 308 32.36 70.04 36.11 107.82 141.13 11.3 121.3 0.91 80 187 282.66 240.4 257.94 25 68 50 8.23 21																			19.19	20.98
214 32.6 62.48 35.24 91.24 119.34 9.4 121.3 0.91 102 231 237.29 245.69 265.65 -23 -32 -52 10.88 14 212 31.99 69.75 35.01 104.82 130.96 13.2 126.6 0.9 85 166 319.09 270.76 253.21 -107 -59 -41 50.51 27 190 31.95 67.92 35.49 96.3 116.61 8.1 148.2 0.84 75 156 320.48 234.32 225.33 -130 -44 -35 68.67 23 148 32.93 71.79 36.24 107.85 137.41 8.1 111.1 0.87 49 130 178.12 129.17 145.03 -30 19 3 20.35 12 266 35.03 73.63 37.79 110.4 140.7 8.1 148.2 0.92 113 181 365.54 392.28 323.16 -100 -126 -57 37.42 47 <t< td=""><td></td><td></td><td></td><td></td><td></td><td></td><td></td><td></td><td></td><td></td><td></td><td></td><td></td><td></td><td></td><td></td><td></td><td></td><td>25</td><td>29.6</td></t<>																			25	29.6
212 31.99 69.75 35.01 104.82 130.96 13.2 126.6 0.9 85 166 319.09 270.76 253.21 -107 -59 -41 50.51 27 190 31.95 67.92 35.49 96.3 116.61 8.1 148.2 0.84 75 156 320.48 234.32 225.33 -130 -44 -35 68.67 23 148 32.93 71.79 36.24 107.85 137.41 8.1 111.1 0.87 49 130 178.12 129.17 145.03 -30 19 3 20.35 12 266 35.03 73.63 37.79 110.4 140.7 8.1 148.2 0.92 113 181 365.54 392.28 323.16 -100 -126 -57 37.42 47 308 32.36 70.04 36.11 107.82 141.13 11.3 121.3 0.91 80 187 282.66 240.4 257.94 25 68 50 8.23 21																			14.81	24.14
190 31.95 67.92 35.49 96.3 116.61 8.1 148.2 0.84 75 156 320.48 234.32 225.33 -130 -44 -35 68.67 23 148 32.93 71.79 36.24 107.85 137.41 8.1 111.1 0.87 49 130 178.12 129.17 145.03 -30 19 3 20.35 12 266 35.03 73.63 37.79 110.4 140.7 8.1 148.2 0.92 113 181 365.54 392.28 323.16 -100 -126 -57 37.42 47 308 32.36 70.04 36.11 107.82 141.13 11.3 121.3 0.91 80 187 282.66 240.4 257.94 25 68 50 8.23 21																			27.72	19.44
148 32.93 71.79 36.24 107.85 137.41 8.1 111.1 0.87 49 130 178.12 129.17 145.03 -30 19 3 20.35 12 266 35.03 73.63 37.79 110.4 140.7 8.1 148.2 0.92 113 181 365.54 392.28 323.16 -100 -126 -57 37.42 47 308 32.36 70.04 36.11 107.82 141.13 11.3 121.3 0.91 80 187 282.66 240.4 257.94 25 68 50 8.23 21																			23.33	18.59
266 35.03 73.63 37.79 110.4 140.7 8.1 148.2 0.92 113 181 365.54 392.28 323.16 -100 -126 -57 37.42 47 308 32.36 70.04 36.11 107.82 141.13 11.3 121.3 0.91 80 187 282.66 240.4 257.94 25 68 50 8.23 21																			12.72	2.01
308 32.36 70.04 36.11 107.82 141.13 11.3 121.3 0.91 80 187 282.66 240.4 257.94 25 68 50 8.23 21																			47.47	21.49
																			21.95	16.25
24 01.07 10.00 01.00 100.21 100.2 121.0 0.70 00 220 100.00 271.7 270.0 109 02 20 42.70 20																			25.4	8.7
	J27	34.07	, 4.00	37.70	103.4/	150.7	0.2	141.0	0.73	00	220	105.70	471./	273.0	107	02	20	72.70	20.7	0.7

Table 4Mean average percentage error of each machine learning algorithm for Model-1. The bold numbers represent the lowest MAPE.

	Yield es	timate MA	PE (%)			
ML Algorithm	k = 1	k=2	k = 3	k = 4	k=5	Average MAPE
PLSR	46.81	30.57	24.11	50.08	27.62	35.84
RFR	86.53	35.72	26.48	29.10	29.51	41.47
LR	31.70	33.72	28.88	50.13	33.51	35.59
GBR	72.28	34.22	22.70	46.36	35.55	41.12

out of all the ML algorithms, while the RFR gave the worst estimate (MAPE of 41.47%; Table 4). Even though LR gave the lowest MAPE, the MAPE of the PLS algorithm (MAPE of 35.84%; Table 4) was not far off. This means that depending on the data, either of these algorithms could have given good prediction results.

The box and whisker plot (Fig. 5) shows the error range in the yield estimate for each ML algorithm. The GBR is top skewed and had the lowest variability in predicting yield, with a median of 25.03% and an interquartile range of 28%. The interquartile range was chosen as a measure of the spread of data instead of standard deviation because the small dataset did not display a normal distribution. The LR algorithm had considerable variability, as seen from the boxplot (Fig. 5), with an interquartile range of 38.79%.

Model-2

For Model-2, UAV data from Model-1 (spectral data and tree structural parameters) and the fruit count from images taken from the front side of the trees were given as the input to the ML algorithms. The model was evaluated using the average MAPE to determine the best algorithm. The average MAPE for each algorithm for each k-fold validation is presented in Table 5.

For Model-2, the best yield estimate was obtained using the PLSR algorithm (MAPE of 23.45%; Table 5), while the GBR gave the worst estimate (MAPE of 31.72%; Table 5). Adding the fruit count from the object detection algorithm as an input parameter to Model-1 resulted in better yield estimates in Model-2, with the average MAPE of the best algorithm improving by 34.11% (35.59% to 23.45%).

Table 5

Mean average percentage error of each machine learning algorithm for Model-2.

The bold number represents the lowest MAPE.

	Yield es	timate MA	PE (%)			
ML Algorithm	k = 1	k=2	k=3	k = 4	k=5	Average MAPE
PLSR	18.44	25.98	24.12	35.76	12.97	23.45
RFR	54.97	28.23	23.96	30.48	18.79	31.29
LR	19.16	31.12	29.69	35.02	16.26	26.25
GBR	60.01	29.34	22.16	29.40	17.67	31.72

The box and whisker plot for Model-2 (Fig. 6) shows the error range in the yield estimate for each ML algorithm. A comparison of the boxplots of Model-1 and Model-2 shows the improvement in yield estimation in terms of the reduction in the spread of the estimates. The PLSR had the lowest variability in predicting yield, with a median of 20.66% and an interquartile range of 18.08%. The RFR algorithm had the highest variability, with an interquartile range of 24.29%.

Model-3

For Model-3, UAV data from Model-1 (spectral data and the tree structural parameters) and the fruit count from images taken from both sides of the trees were given as the input to the ML algorithms. Like the previous models, evaluation was done using average MAPE to determine the best algorithm. The average MAPE for each algorithm for each of the k-fold validation for Model-3 is presented in Table 6. For Model-3, like Model-2, the PLSR algorithm gave the best results (MAPE of 25.72%; Table 6), while the RFR performed the worst in terms of prediction accuracy (MAPE of 37.78%; Table 6).

The box and whisker plot for Model-3 (Fig. 7) shows the error range in the yield estimate for each ML algorithm. A comparison of all the boxplots reveal that Model-2 and Model-3 perform better than Model-1 in terms of the reduction in spread of yield estimates. For Model-3, the LR algorithm had the lowest variability in predicting yield, with a median of 30.31%, and an interquartile range of 15.11%. The RFR algorithm had the highest variability with an interquartile range of 28.27%.

Model Comparison

Even though Model-3 included the fruit count from images taken

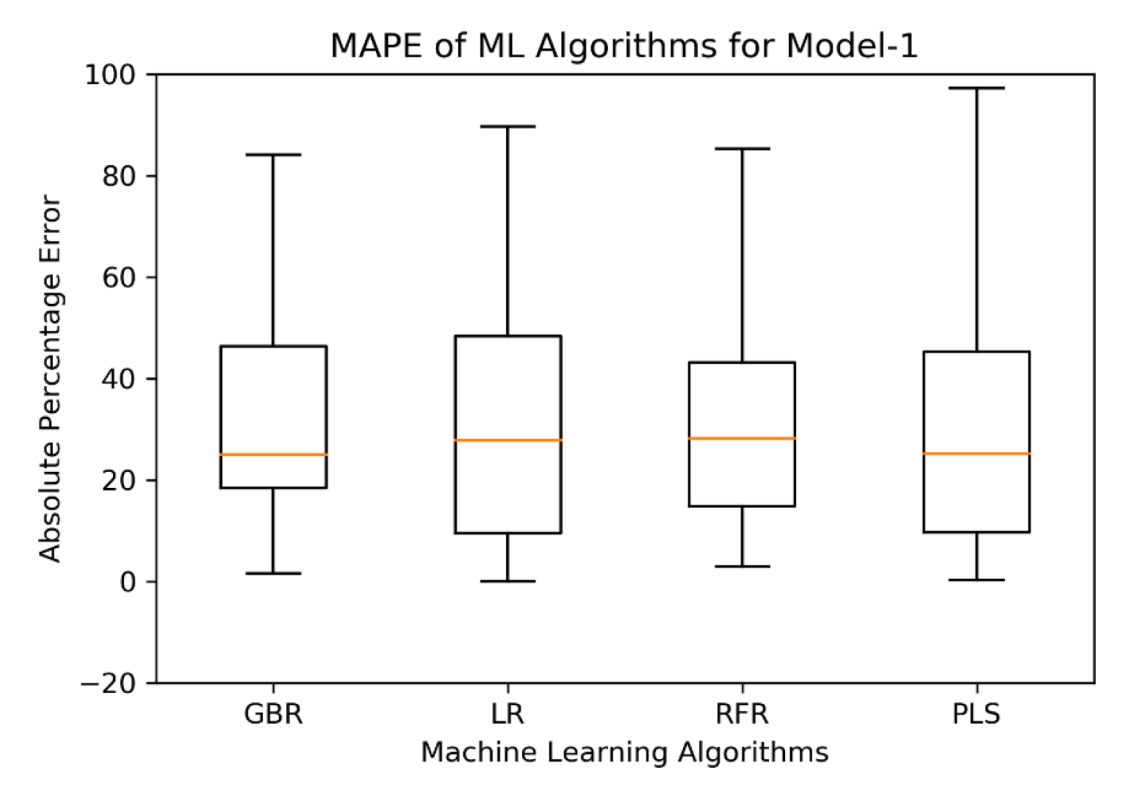


Fig. 5. Boxplot of MAPE for Model-1.

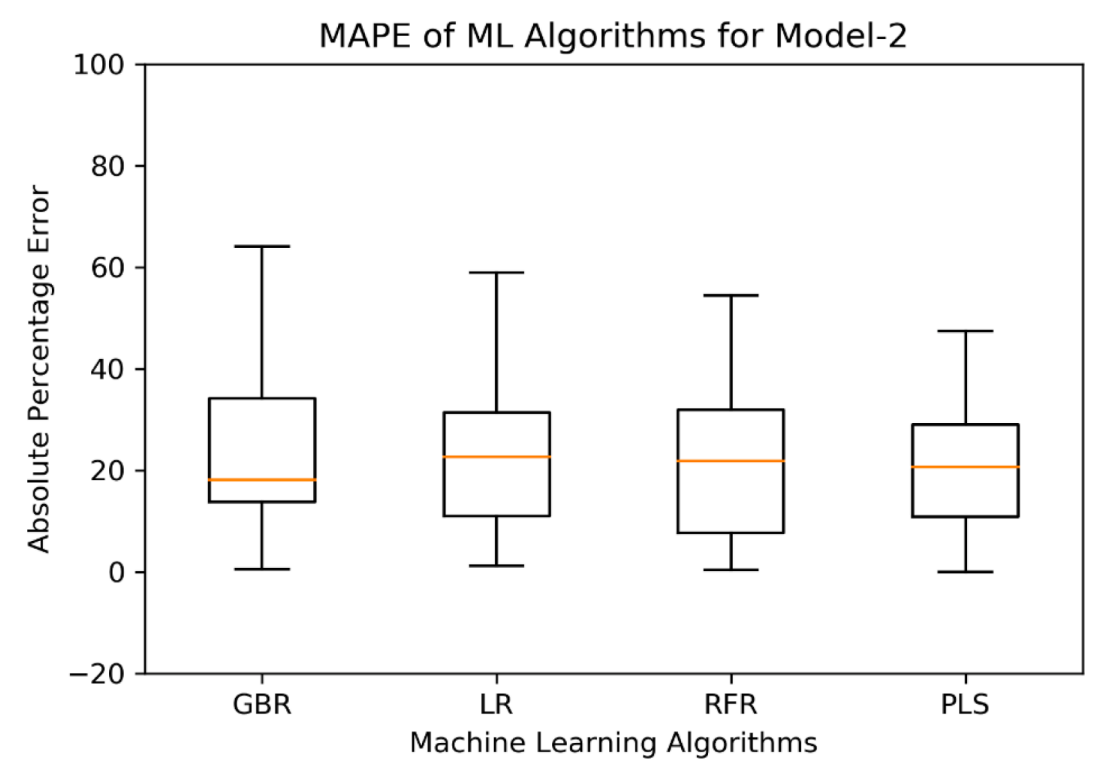


Fig. 6. Boxplot of MAPE for Model-2.

Table 6Mean average percentage error of each machine learning algorithm for Model-3. The bold number represents the lowest MAPE.

	Yield es	timate MA	PE (%)			
ML Algorithm	k = 1	k=2	k = 3	k = 4	k=5	Average MAPE
PLSR	26.99	25.42	23.36	40.26	12.55	25.72
RFR	65.90	28.65	34.01	39.39	20.93	37.78
LR	31.54	27.58	30.12	45.77	16.55	30.31
GBR	70.06	29.43	25.21	28.16	13.98	33.37

from both sides of the tree in the object detection algorithm as an input parameter as opposed to just the one-sided image in Model-2, it was found that the best ML algorithm of Model-3 has a higher MAPE (25.72%) as compared to the best ML algorithm of Model-2 (23.45%).

All the algorithms, when applied on Model-2, gave a MAPE less than 32%, while for Model-3, except for PLS, all other algorithms gave a MAPE of more than 30% indicating the fact that Model-2 gave the overall lowest error in yield prediction. The two best-performing algorithms for both these models, PLS and LR, had a lower variability in the case of Model-3 as compared to Model-2, while the two worst-performing models, GBR and RFR, had much greater variability in Model-3, as indicated by their boxplots (Figs. 6 and 7).

The lower MAPE of Model-2 and Model-3 shows that they are more accurate than Model-1 in terms of yield prediction (at the tree level). Tests for statistical significance performed on these three models using paired t-tests suggested a significant difference between Model-1 and Model-2 (p-value = 0.0013), Model-1 and Model-3 (p-value = 0.0010), but no significant difference between Model-2 and Model-3 (p-value = 0.29).

4. Discussion

4.1. Accuracy of the fruit detection model

The fruit detection using YOLO v3 gave a high precision of 0.96, a

recall of 0.83, and an average F1 score of 0.88, suggesting a good fruit detection model. Since the object detection model involved transfer learning using a weight file previously trained on immature citrus fruits, the detection accuracy was high. This could be further improved with more images of mature citrus fruits taken from multiple farms at different times of the day. However, these models still would not be able to accurately detect all the fruits because of the occlusion of the fruits by leaves and branches. The algorithm uses multiple parameters such as color, contour, texture, and other features for detection. Many variables such as the camera specifications, time of the image taken, and shadows affect the quality of the image and overall detection. However, the main objective of this model is not to count all fruits in a tree, rather than to get an estimate of fruit count to be used for the yield prediction models presented in this study.

4.2. Machine learning models applied for yield estimation

Model-1

All the yield prediction algorithms had multiple outliers, with an error estimate for some outliers of over 100%. Closer inspection of the data revealed that those outliers belonged to smaller trees with less than 100 fruits (fruit counts of 61, 87, 92, and 44). These trees had a height comparable to the larger trees and a canopy area proportional to their harvest output. This variability in tree size and fruit load could be because of the different rootstock varieties used in this field. However, the spectral values were similar in range to that of a larger tree (trees with medium (100< fruit count <350) or large harvest numbers (>350)). This indicates that yield estimation based only on the spectral data is unreliable for smaller trees (fruit count less than 100). Hence, a model that includes fruit counts as an input parameter could theoretically provide a better yield estimation than Model-1. For trees with larger harvest outputs, Model-1 performed better than Model-2 in only 2 $\,$ out of 7 (28.5%) cases (Table 8). The relatively poor performance of Model-1 compared to Model-2 and Model-3 could be because of the effect of the weather conditions, the intensity of sunlight, and the variations in brightness during the process of UAV image acquisition which

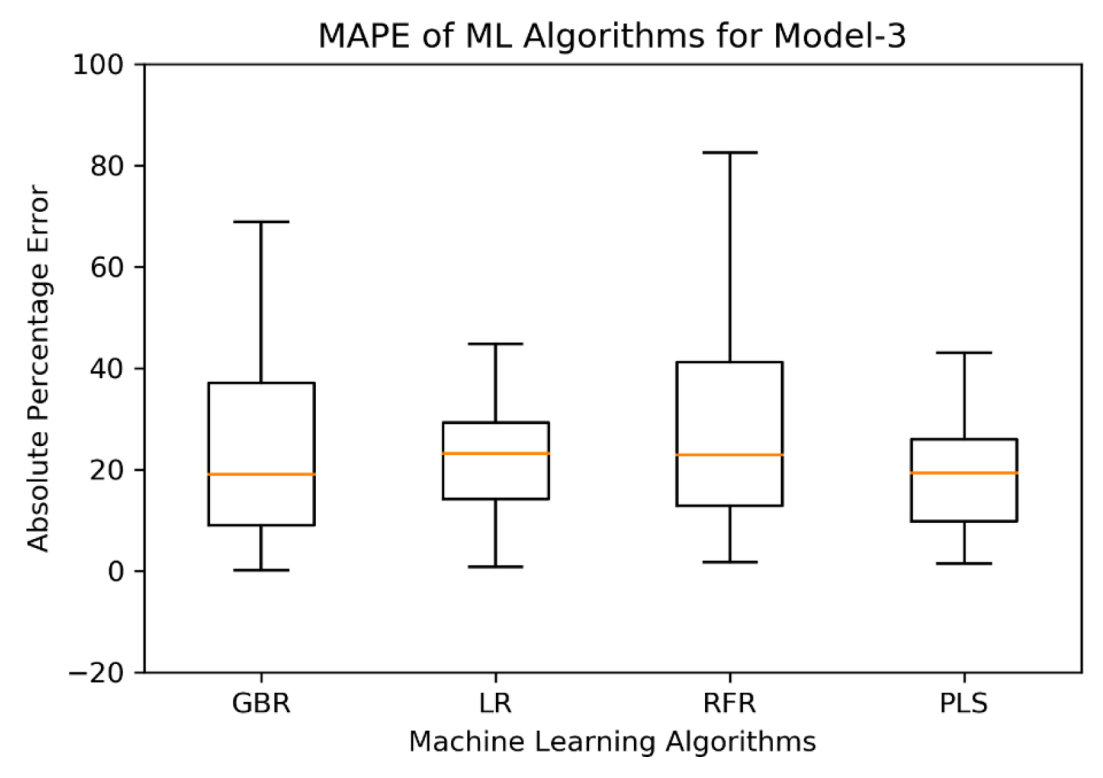


Fig. 7. Boxplot of MAPE for Model-3.

could have affected the multispectral values.

Model-2

The yield estimate for each ML algorithm used in Model-2 was better (Fig. 6) than in Model-1. Overall, the yield estimate for almost all the trees improved as the variability in yield estimate decreased and the median value for all the algorithms was reduced to less than 23%. There was also a remarkable drop in the mean value of the yield estimate for all the algorithms, with every ML algorithm giving under 32% average MAPE.

For trees with a yield per tree (harvest) count of fewer than 100 fruits, Model-2 gave a far better yield prediction than Model-1 in almost every case (Table 7). Compared to Model-1, Model-2 showed a reduction in error of at least 40% in three out of four cases (75%) of smaller trees (Table 7). Model-2 also had the best root mean square error (RMSE) (54.64) of the predictions for smaller trees as compared to Model-1 (102.77) and Model-3 (79.07). For trees with higher fruit load (greater than 350 fruits per tree), Model-2 still performed better in 5 out of 7 cases (71.4%) (Table 8). This showed that including fruit count, even from a single side of the tree, in the model improved the yield estimation for both the smaller and larger trees.

Model-3

Model-3 performed better than Model-1 and similar or worse than Model-2 for all four algorithms. This could be because of the double counting of fruits when using the fruit count of images from both sides of a tree. Double counting results in overestimating fruits (higher "2-side count" in Table 1), especially when the tree leaf density is low. For

Table 7Absolute percentage error (APE) of each Model for trees with a harvest count of less than 100 fruits.

	Absolute Perce	ntage Error	
Harvest Count	Model-1	Model -2	Model-3
61	25.11	32.69	21.51
87	191.86	97.09	145.64
92	131.98	71.52	93.14
44	89.7	20.66	86.16

Table 8
Absolute percentage error (APE) of each Model for trees with a harvest count of more than 350 fruits.

Harvest Count	Absolute Percentage Error							
	Model-1	Model -2	Model-3					
442	3.89	2.58	2.91					
412	16.99	23.82	15.45					
362	27.77	13.54	14.75					
387	50.07	21.77	31.79					
439	34.12	28.42	24.44					
368	1.68	13.88	6.43					
409	38.44	11.68	14.19					

smaller trees, Model-3 performed better than Model-1 in all the cases, as is evident from the lower APE values (Table 7). Even in the case of trees with larger harvest output, Model-3 gave lower APE in 6 out of 7 (85.7%) cases as compared to Model-1 and in 3 out of 7 (42.8%) cases as compared to Model-2 (Table 8). This shows that using the fruit count from one side (Model-2) is a better alternative to using fruit count from images taken from both sides of the tree.

Model Comparison

The comparison of models based on MAPE suggests the use of Model-2 for a more accurate yield estimation at a tree level. Model-2 gave the lowest MAPE (MAPE of 23.45%) compared to the other two models. The statistical significance tests showed a significant difference between the yield prediction errors of Model-1 and Model-2, and Model-1 and Model-3. Between Model-2 and Model-3, even though the difference in MAPE was around 2%, the difference was not statistically significant. This indicates that using either of Model-2 and Model-3 would be a better choice than Model-1. This conclusion works in favor of Model-2 being used as a yield estimation model over Model-3, because Model-2 requires less input data; Model-2 would be less taxing in terms of the time and effort required to capture images from only one side of the tree. It would also be more scalable when used in large commercial fields, where a camera mounted on a farm vehicle could be used for capturing a video of one side of the citrus trees while traversing through the rows.

The captured video could then be used for extracting images for fruit count from one side and subsequently serve as an input to Model-2.

The UAV imagery was important in extracting the spectral values and the structural parameters (through Agroview) of trees. Model-2 and Model-3 without any UAV data showed a higher variance in data (data not presenting in this paper), suggesting that using both UAV and ground-based data was more reliable than just using ground-based data. Aerial data can be captured through a UAV much faster for a larger area of the field. The bottleneck might arise while capturing ground data through a camera mounted on a farm vehicle driving slowly between the rows. This could be problematic if the rows of trees are too close and there are spatial restrictions on driving a farm vehicle to capture the entire canopy of the tree from one side.

At a block level (experimental area of 48 citrus trees), all three models predicted yield with more than 99% accuracy. However, a large-scale experiment, with a high number of trees, is needed to better evaluate the performance of the models. In large-scale experiments (e.g., 5,000 trees total), it is very difficult to collect yield data for each individual tree, but the comparison of the model at a block (e.g., specific area in a farm) level is possible. The performance of the models should be also tested in different locations and during different dates before harvest.

5. Conclusion

Existing yield prediction methods either use UAVs to predict yield from canopy parameters and spectral imaging, or use ground images only for fruit counting without estimating actual yield. This study compares the yield prediction (at a tree level) from three different MLbased models. The first model (Model-1) includes data collected from UAV imagery. The second and third models utilize UAV imaging along with fruit count derived from a deep learning algorithm applied to images taken from one side (Model-2) and both sides (Model-3) of the tree. The average MAPE calculation revealed that the models that included the fruit count performed better than the model that just used the UAV data. Model-2, which used fruit count from only one side of the tree, performed similarly with Model-3, which included fruit count from both sides of the tree. Model-2 was selected as a desired model because of the less input data required for yield prediction (compared to Model-3). In general, the results demonstrate that the developed Model-2 could be used to predict the fruit count in orange orchards in Florida.

The selected model, Model-2, gave a MAPE of 23.45%. Model-2 also estimated the yield better for trees with the smallest and largest fruit load (harvest count less than 100 and more than 350 fruits, respectively) as compared to Model-1 and Model-3. These results support the development of models using UAV multispectral imaging and fruit count via image-based fruit detection (images taken from the ground). A model including UAV collected spectral data and fruit count information would help reduce the overall error in the traditional yield estimation process, which is manual as of now in many citrus farms in Florida, and ultimately reduce the financial losses of growers. Future works will involve improving the detection accuracy of the fruit detection system by using more advanced robust networks. These models would use images from immature fruits for training and validation and perform prediction 4-6 months in advance of harvesting. Capturing tree images using UAVs flown closer to one side of the trees could be used as an alternative to ground-based image capture for regions where it is difficult to drive farm vehicles in between rows. Future work will also include an evaluation of the estimation performance and cost analysis of the object detection and UAV based models in comparison with the existing manual methods of fruit prediction.

Declaration of competing interests

The authors declare that they have no known competing financial interests or personal relationships that could have appeared to influence the work reported in this paper.

Acknowledgement

This material was made possible, in part, by a Cooperative Agreement from the U.S. Department of Agriculture's Animal and Plant Health Inspection Service (APHIS) and Agricultural Marketing Service through grant AM190100XXXXG036. Its contents are solely the responsibility of the authors and do not necessarily represent the official views of the USDA."

References

- [1] Y.G. Ampatzidis, S.G. Vougioukas, Field experiments for evaluating the incorporation of RFID and barcode registration and digital weighing technologies in manual fruit harvesting, Comput. Electron. Agric. 66 (2) (2009) 166–172, https://doi.org/10.1016/J.COMPAG.2009.01.008.
- [2] Y. Ampatzidis, V. Partel, UAV-based high throughput phenotyping in citrus utilizing multispectral imaging and artificial intelligence, Remote Sensing 11 (4) (2019), https://doi.org/10.3390/rs11040410.
- [3] Y. Ampatzidis, V. Partel, L. Costa, Agroview: Cloud-based application to process, analyze and visualize UAV-collected data for precision agriculture applications utilizing artificial intelligence, Comput. Electron. Agric. 174 (2020), 105457, https://doi.org/10.1016/j.compag.2020.105457.
- [4] Y. Ampatzidis, L. Tan, R. Haley, M.D. Whiting, Cloud-based harvest management information system for hand-harvested specialty crops, Comput. Electron. Agric. 122 (2016) 161–167, https://doi.org/10.1016/J.COMPAG.2016.01.032.
- [5] Y.G. Ampatzidis, S.G. Vougioukas, M.D. Whiting, Q. Zhang, Applying the machine repair model to improve efficiency of harvesting fruit, Biosystems Eng. 120 (2014) 25–33, https://doi.org/10.1016/J.BIOSYSTEMSENG.2013.07.011.
- [6] Anderson, N. T., Underwood, J. P., Rahman, M. M., Robson, A. & Walsh, K. B. (2019). Estimation of fruit load in mango orchards: tree sampling considerations and use of machine vision and satellite imagery. *Precision Agriculture*, 20, 823–839. https://doi.org/10.1007/s11119-018-9614-1.
- [7] O.E. Apolo-Apolo, J. Martínez-Guanter, G. Egea, P. Raja, M. Pérez-Ruiz, Deep learning techniques for estimation of the yield and size of citrus fruits using a UAV, Eur. J. Agron. 115 (2020), https://doi.org/10.1016/J.EJA.2020.126030.
- [8] Begeman, J., & Wright, G. (2009). Diagnosing Home Citrus Problems.
- [9] P. Benedetti, D. Ienco, R. Gaetano, K. Ose, R.G. Pensa, S. Dupuy, M 3 fusion: a deep learning architecture for multiscale multimodal multitemporal satellite data fusion, IEEE J. Sel. Topics Appl. Earth Observ. Remote Sens. 11 (12) (2018) 4939–4949, https://doi.org/10.1109/JSTARS.2018.2876357.
- [10] J. Brownlee, A Gentle Introduction to the Gradient Boosting Algorithm for Machine Learning, Mach. Learn> Mastery (2016) 1–21. https://machinelearningmastery. com/gentle-introduction-gradient-boosting-algorithm-machine-learning/.
- [11] J. Brownlee, A gentle introduction to soar, An Invitation Cognit. Sci. (2019) 1, https://doi.org/10.7551/mitpress/3967.003.0009.
- [12] Choi, D., Lee, W. S., Schueller, J. K., Ehsani, R., & Roka, F. (2017). An ASABE Meeting Presentation A performance comparison of RGB, NIR, and depth images in immature citrus detection using deep learning algorithms for yield prediction. https:// doi.org/10.13031/aim.201700076.
- [13] L. Costa, Y. Ampatzidis, C. Rohla, N. Maness, B. Cheary, L. Zhang, Measuring pecan nut growth utilizing machine vision and deep learning for the better understanding of the fruit growth curve, Comput. Electron. Agric. 181 (2021), https://doi.org/ 10.1016/J.COMPAG.2020.105964.
- [14] Costa, L., McBreen, J., Ampatzidis, Y., Guo, J., Reisi Gahrooei, M., & Ali Babar, M. (1234). Using UAV-based hyperspectral imaging and functional regression to assist in predicting grain yield and related traits in wheat under heat-related stress environments for the purpose of stable yielding genotypes. https://doi.org/10.1007/s11119-021-09852-5.
- [15] Court, C. D., Ferreira, J., & Cruz, J. (2018). ECONOMIC CONTRIBUTIONS of the FLORIDA CITRUS INDUSTRY Sponsored project report to the Florida Department of Citrus.
- [16] I. Díaz, S.M. Mazza, E.F. Combarro, L.I. Giménez, J.E. Gaiad, Machine learning applied to the prediction of citrus production, Spanish J. Agricult. Res. 15 (2) (2017), https://doi.org/10.5424/sjar/2017152-9090.
- [17] B. Diennevan, S. Barbosa, G. Araújo, S. Ferraz, L. Costa, Y. Ampatzidis, V. Vijayakumar, L. Mendes, D. Santos, UAV-based coffee yield prediction utilizing feature selection and deep learning, Smart Agricult. Technol. 1 (2021), 100010, https://doi.org/10.1016/J.ATECH.2021.100010.
- [18] Y. Everingham, J. Sexton, D. Skocaj, G. Inman-Bamber, Accurate prediction of sugarcane yield using a random forest algorithm, Agron. Sustainable Dev. 36 (2) (2016). https://doi.org/10.1007/s13593-016-0364-z.
- [19] A. Kayad, M. Sozzi, S. Gatto, F. Marinello, F. Pirotti, Monitoring within-field variability of corn yield using sentinel-2 and machine learning techniques, Remote Sensing (23) (2019) 11, https://doi.org/10.3390/rs11232873.
- [20] S. Khaki, L. Wang, S.V. Archontoulis, A CNN-RNN Framework for Crop Yield Prediction, Front. Plant Sci. 10 (January) (2020) 1–14, https://doi.org/10.3389/ fols.2019.01750.
- [21] \vec{A} . Koirala, · K B Walsh, · Z Wang, · C Mccarthy, * A Koirala, Deep learning for real-time fruit detection and orchard fruit load estimation: benchmarking of

- "MangoYOLO.", Precis. Agricult. 20 (2019) 1107–1135, https://doi.org/10.1007/
- [22] K. Kuwata, R. Shibasaki, Estimating corn yield in the United States with modis EVI and machine learning methods, ISPRS Ann. Photogrammetry Remote Sensing Spatial Inf. Sci. III–8 (2016) 131–136, https://doi.org/10.5194/isprsannals-iii-8-131-2016.
- [23] M. Maimaitijiang, A. Ghulam, P. Sidike, S. Hartling, M. Maimaitiyiming, K. Peterson, E. Shavers, J. Fishman, J. Peterson, S. Kadam, J. Burken, F. Fritschi, Unmanned Aerial System (UAS)-based phenotyping of soybean using multi-sensor data fusion and extreme learning machine, ISPRS J. Photogramm. Remote Sens. 134 (2017) 43–58, https://doi.org/10.1016/J.ISPRSJPRS.2017.10.011.
- [24] Minitab Support. (2017). What is partial least squares regression?1. https://support.minitab.com/en-us/minitab/18/help-and-how-to/modeling-statistics/regression/supporting-topics/partial-least-squares-regression/what-is-partial-least-squares-regression/.
- [25] Mviti, D. (2020). Random Forest Regression when does it fail and why (pp. 1–9). https://neptune.ai/blog/random-forest-regression-when-does-it-fail-and-why.
- [26] Ngiam, J., Khosla, A., Kim, M., Nam, J., Lee, H., & Ng, A. Y. (2011). Multimodal Deep Learning.
- [27] Nunes, L., Ampatzidis, Y., Costa, L., & Wallau, M. (2021). Horse foraging behavior detection using sound recognition techniques and artificial intelligence. *Computers and Electronics in Agriculture*, 183. https://doi.org/10.1016/J. COMPAG.2021.106080.
- [28] V. Partel, L. Costa, Y. Ampatzidis, Smart citrus tree sprayer using sensor fusion and artificial intelligence Written for presentation at, in: the 2021 Annual International Meeting ASABE Virtual and On Demand, 2021, https://doi.org/10.13031/ aim. 2021.00525
- [29] Python, R. (2020). Linear regression in python real python. 1–21. https://realpython.com/linear-regression-in-python/.
- [30] Redmon, J., & Farhadi, A. (2018). YOLOv3: An Incremental Improvement. htt p://arxiv.org/abs/1804.02767.
- [31] P. Rischbeck, S. Elsayed, B. Mistele, G. Barmeier, K. Heil, U. Schmidhalter, Data fusion of spectral, thermal and canopy height parameters for improved yield

- prediction of drought stressed spring barley, Eur. J. Agron. 78 (2016) 44–59, https://doi.org/10.1016/j.eja.2016.04.013.
- [32] B. Russell, A. Torralba, W.T. Freeman, Labelme: the open annotation tool, Comput. Sci. Artif. Intell. Lab. (2006) [Online]. Available: Http://Labelme. Csail. Mit. Edu. http://labelme.csail.mit.edu/guidelines.html.
- [33] Sarron, J., Malézieux, É., Amet, C., Sané, B., & Faye, É. (2018). Remote sensing mango yield mapping at the orchard scale based on tree structure and land cover assessed by UAV. https://doi.org/10.3390/rs10121900.
- [34] J.K. Schueller, Opinion: opportunities and limitations of machine vision for yield mapping, Front. Rob. AI 8 (2021), https://doi.org/10.3389/frobt.2021.627280.
- [35] Scikit-learn. (2020). Gradient Boosting regression. https://scikit-learn.org/stable/auto_examples/ensemble/plot_gradient_boosting_regression.html.
- [36] A.X. Wang, C. Tran, N. Desai, D. Lobell, S. Ermon, Deep transfer learning for crop yield prediction with remote sensing data, in: Proceedings of the 1st ACM SIGCAS Conference on Computing and Sustainable Societies, COMPASS 2018 18, 2018, https://doi.org/10.1145/3209811.3212707.
- [37] C. Wang, Won, S. Lee, Xiangjun Zou, D. Choi, Hao Gan, Justice, X Zou, Detection and counting of immature green citrus fruit based on the Local Binary Patterns (LBP) feature using illumination-normalized images, Precis. Agricult. 19 (2018) 1062–1083, https://doi.org/10.1007/s11119-018-9574-5.
- [38] ichi X. Ye, K. Sakai, S. Asada, A. Sasao, Application of narrow-band TBVI in estimating fruit yield in citrus, Biosystems Eng. 99 (2) (2008) 179–189, https:// doi.org/10.1016/J.BIOSYSTEMSENG.2007.09.016.
- [39] X. Ye, K. Sakai, A. Sasao, S.I. Asada, Estimation of citrus yield from canopy spectral features determined by airborne hyperspectral imagery, Int. J. Remote Sens. 30 (18) (2009) 4621–4642, https://doi.org/10.1080/01431160802632231.
- [40] Q.U. Zaman, A.W. Schumann, H.K. Hostler, Estimation of citrus fruit yield using ultrasonically-sensed tree size, Appl. Eng. Agric, 22 (1) (2006) 39–44.
- [41] X. Zhang, A. Toudeshki, R. Ehsani, H. Li, W. Zhang, R. Ma, Yield estimation of citrus fruit using rapid image processing in natural background, Smart Agricult. Technol. 2 (2022), 100027, https://doi.org/10.1016/j.atech.2021.100027.